Correlations of power output fluctuations in an offshore wind farm using high-resolution SCADA data

Janna K. Seifert[1], Martin Kraft[1,], Martin Kühn[1,], and Laura J. Lukassen[1]

[1]ForWind, Institute of Physics, Carl von Ossietzky University Oldenburg, Küpkersweg 70, 26129 Oldenburg, Germany

Correspondence: Janna K. Seifert (janna.kristina.seifert@uol.de)

Abstract. The correlation of power output fluctuations of wind turbines in free field are investigated, taking into account the challenge of varying correlation states due to variable flow and wind turbine conditions within the wind farm. Based on eight months of 1 Hz SCADA data, measured at an offshore wind farm with 80 wind turbines, the influence of different parameters on the correlation of power output fluctuations is analysed. It is found that the correlation of power output fluctuations of wind

5 turbines depends on the location of the wind turbines within the wind farm as well as the inflow conditions (free-stream or wake). Wind direction investigations show that the correlation is highest for streamwise aligned pairs and decreases towards spanwise pairs. Most importantly, the highly variable measurement data in a free-field wind farm has considerable influence on the identification of different correlation states. To account for that, the clustering algorithm k-means is used to group wind turbine pairs with similar correlations. The main outcome is that next to the location of a wind turbine pair in the wind farm

10 the standard deviation in their power output and their power differences are suitable parameters to describe the correlation of power output fluctuations.

1 Introduction

Wind energy continues to be a growing source of energy. In 2019, 15.4 GW of new wind power capacity was installed in Europe, 24 % thereof offshore (WindEurope, 2020a). Considering offshore wind power in 2019, the capacity in Europe has

15 increased by 3.627 GW, and a total of 7 wind farms were connected to the grid, and the average size of wind farms increased to 621 MW (WindEurope, 2020b).

With the continuously increasing share of wind energy in the grid, the challenge of handling this highly fluctuating energy source becomes more important as discussed in Ren et al. (2017). To convert wind energy into electrical energy, wind turbines are installed, generally in groups (wind farms) at onshore and offshore sites. Fluctuations in their power output are the result

20 of environmental influences such as changes in wind speed or wind direction, influences from neighbouring wind turbines, but also their own state of operation. These power output fluctuations create challenges regarding the grid stability and therefore are an important field of investigation, (cf. Sorensen et al., 2007; Bossuyt et al., 2017b).

In order to achieve the maximum power output for the respective site, wind turbines within a wind farm are placed as efficiently as possible. The spacing of wind turbines is determined by the terrain of the site and the influence of wind turbines onto

25 each other (their wake). Wakes cause energy losses through reduced wind speeds and at the same time greater power output

fluctuations and loads through increased turbulence (Crespo and Hernàndez, 1996; Vermeer et al., 2003).

Wake and wind farm flow effects on different spatial and temporal scales are reviewed by Porté-Agel et al. (2020). Many studies do not take power output fluctuations of wind turbines into account which have a high impact on the power output of a wind farm and the electrical grid. Thus, for further improvement of wind turbine control strategies like active power control

30 (Vali et al., 2019) and grid stability by minute-scale prediction of offshore wind farm power (Valldecabres et al., 2020), the occurrence of wind turbine power output fluctuations and their correlation within a wind farm are of great interest.

Andersen et al. (2017) investigated the influence of large coherent structures on the power output of wind turbines in large wind farms. They were found to cause a high correlations in the power output of streamwise aligned wind turbines. Research on wind speed correlations and power output correlations has shown that wind turbines within a wind farm influence each other's power

35 output fluctuations. Bossuyt et al. (2017a) showed that for a wind farm of 100 porous disc models in a wind tunnel, significant correlations of the power output can be found for a streamwise aligned set up of the discs. Next to an increased turbulence intensity throughout the wind farm, the correlation of the power output reduced with increasing distance of the discs to each other. In an LES study by Lukassen et al. (2018) velocity space-time correlations within an infinitely large wind farm were analysed and modelled analytically. The velocity fluctuations which are directly related to power output fluctuations showed

40 pronounced space-time correlations. Furthermore, the variance of the wind velocity turned out to be an important parameter in the modelling set up. Stevens and Meneveau (2014) investigated spectra of wind turbine power output fluctuations in LES of finitely sized and infinitely large wind farms. The spectra were found to be depended on non-trivial correlations of streamwise placed wind turbines. The correlation of two wind turbines was significantly influenced by the wind direction, i.e. lowest correlation for spanwise placed wind turbines and highest correlation for streamwise aligned wind turbines. Dai et al. (2017)

45 analysed 1 Hz wind farm SCADA data with respect to the influence of wind speed fluctuations and wind direction fluctuations on wind turbine power output fluctuations of single wind turbines. They showed a direct relation of wind speed fluctuations and power output fluctuations in the partial load regime whereas wind direction fluctuations have only little effect. By using 10 minute averaged wind farm SCADA data, Braun et al. (2020) derived a stochastic model for the power time series of wind turbines which was based on the temporal autocorrelation of single wind turbines.

50 In our work, we analyse 1 Hz wind farm SCADA data to describe space-time correlations of power output fluctuations of wind turbine pairs. In contrast to the wind tunnel measurements by Bossuyt et al. (2017a) and the LES analysis by Lukassen et al. (2018) mentioned above, the data set processed here includes unstable inflow conditions, dynamically operating wind turbines as well as changing flow conditions within the wind farm. Furthermore, there may be potential measurement inaccuracies. The result is a highly complex data set. In this paper we investigate the influence factors which determine different correlation

55 states. For that we group the correlations based on wind turbine statistics.

Starting with the description of the evaluated data set in Sect. 2, the processing of the data is explained in Sect. 2.1 and 2.2. The space-time correlation of power output fluctuations per wind turbine pair for time intervals of 600 s is introduced. Using a filtered data set with less varying flow conditions, the correlations are analysed for different wind directions in Sect. 3.1. The correlation for wind directions with streamwise aligned wind turbines is evaluated in more detail. In Sect. 3.2, the location

60 dependency of the power output fluctuation correlation is determined by the comparison of wind turbine pairs located in

different wind farm rows to confirm the findings of the wind tunnel measurements by Bossuyt et al. (2017a). With this and the results from the LES analysis by Lukassen et al. (2018), we identify relevant wind turbine statistics which influence the correlation. In Sect. 4 we use the straightforward k-means clustering approach (Lloyd, 1982) to group the data with respect to these statistical quantities and show that there are clearly distinguishable correlation states. Conclusion and an outlook are

65   drawn in Sect. 5.

2   Reference wind farm and data processing

The analysis performed in this work is based on measurements from the offshore wind farm Global Tech I (GT I). It is located in the North Sea more than 100 km off the coast of Northern Germany. Its total capacity of 400 MW is provided by 80 wind turbines spread over an area of about 41 km^2. The wind turbines of type Adwen AD 5-116 have a rated power of 5 MW, a

70   rated wind speed of 12.5 ms^{-1}, a hub height of 92 m and a rotor diameter (D) of 116 m. They are installed in a grid like, non-axisymmetric pattern with a triangular shape towards south (see Fig. 1).

The analysed data set was measured in a period of about eight month, from January 1st, 2019 until September 9th, 2019 and consists of 1 Hz wind turbine SCADA data. The processed signals include the generated power P, the azimuth angle of the wind turbine (i.e. the nacelle direction) θ, the nacelle based wind direction φ (measured relative to θ), the pitch angle β of each

75   blades, and the nacelle based wind speed U. It has to be noted that the wind speed U is not directly measured but recalculated from the measured power and the control settings of the wind turbine. Due to that, U is an approximated and idealised value which does not include wind speed independent power reduction, e.g. by misalignment of the wind turbine. However, it can
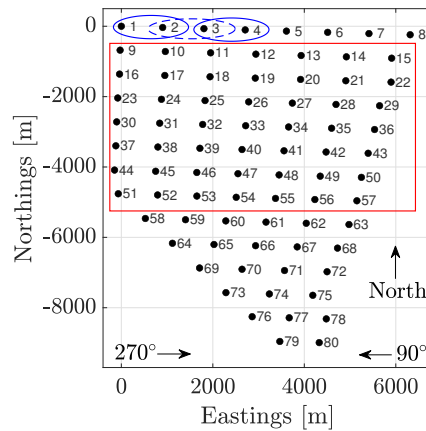
Figure 1. Layout of GT I. Each wind turbine is labelled with its corresponding number. The spacing of the wind turbines is inhomogeneous. The wind directions 90° and 270° (marked in the figure) will be analysed in detail in the subsequent sections. The red square depicts the set of wind turbines which will later be used during the location-dependency analysis in Sect. 3.2 due to their symmetric arrangement. In the clustering analysis in Sect. 4 the whole wind farm will be used. The blue ellipses exemplarily show the definition of streamwise wind turbine pairs. The definition of all pairs is listed in Tab. A1.

still be used for assessing the effect of the wind speed on the wind turbine. The azimuth angle θ of the wind turbine refers to the direction it is facing in its preset reference system. This system does not necessarily exactly match to the global geographical

80 one due to the measurement inaccuracies of the azimuth angle and a potentially inaccurate north orientation of the reference system of each wind turbine (cf. Bromm et al.). The nacelle based wind direction φ is estimated based on the measurements of two 2D sonic anemometers installed behind the rotor of each wind turbine. These measurements have to be treated with care as the measured flow behind the rotor is disturbed by the rotation of the rotor and the nacelle itself. Thus, it is only an estimation of the wind direction facing the wind turbine. The combined measurements of θ_i and φ_i define the wind direction Φ_i facing

85 the i-th wind turbine.

For assessing an average wind direction for the wind farm, we average over Φ_i of all wind turbines. Due to the size of the considered wind farm, the wind direction is not expected to be consistent throughout the whole wind farm. Single wind turbines could still be facing different wind directions compared to the average wind direction of the wind farm (cf. Schneemann et al., 2020; Sanchez Gomez and Lundquist, 2020). The average wind direction over all available wind turbines is defined as Φ_{av}.

90 ## 2.1 Filtering

Wind tunnel experiments and LES simulations as described in Sect. 1, pose controllable conditions for evaluating correlations. Such conditions can not be met in a free-field wind farm. Next to temporally and spatially varying wind conditions, the layout of the wind farm leads to unequal conditions to wind turbines due to their positions, e.g. changing wind direction throughout the wind farm, especially for large wind farms. Further, each wind turbine is acting independently of the other wind turbines

95 including yawing, pitching, start up or shut down. Next to this, single wind turbines can be set to operate in a down-rated state or be shut down due to maintenance or other reasons. All these factors multiply to an order of unpredictable variability within a wind farm which causes highly dynamical flow conditions. To cope with these issues, the data set is filtered for reasonable parameters, which limits the variability in the data set. For each $600\,\mathrm{s}$ interval, the parameters defined in the following have to be met, cf. Tab. 1. Depending on the operational state of a wind turbine, the power output fluctuation characteristics and the

100 influence on other wind turbines changes. Therefore, the data set is filtered for different operation states creating a cleaned data set with comparable operation state conditions for all wind turbines.

In general, a wind turbine operating in partial load is not pitching and the velocity in its wake is always below rated wind speed. A wind turbine operating in full load aims at keeping a constant rotor speed and power by pitching its blades, where the wind speed in its wake can be larger than rated wind speed. To avoid the effects of pitching and the different wake behaviour

105 on the correlation of wind turbines, the data set is limited to partial load. To further avoid effects from the transition from idle

Table 1. Filters applied to the raw data of each wind turbine within the wind farm.

Signal	Power	Pitch	Yaw
Settings	$0.5\,\mathrm{MW} \leq P \leq 4.5\,\mathrm{MW}$	$\beta < -1.3°$	no yawing

mode into operation or the transition from partial load to full load, only the data of wind turbines generating power in the range of 0.5 MW and 4.5 MW is considered.

The previously defined, limited power range still includes derated wind turbines. Wind turbines being derated means that the maximum power of the wind turbines is limited to a certain value lower than their rated power. Due to that wind turbines might

110 start pitching already in the previously defined load range. To fully exclude pitching wind turbines, the data is filtered for any pitching activity, only allowing pitch values smaller than -1.3°.

Furthermore, yawing wind turbines are excluded from the analysis as well. The adjustment of wind turbines to the wind direction is managed by each wind turbine individually. Thus, wind turbines could be facing slightly different wind directions Φ_i and start yawing at different times. The yawing activity of a wind turbine transfers to its wake, i.e. changes its deflection

115 (cf. Bromm et al.). This would affect the correlation of two wind turbines. To exclude yawing wind turbines, no change of θ is allowed in the regarded 600 s time interval.

To further filter the data for wind directions, the average wind direction Φ_{av} of all wind turbines is calculated for each time step of the regarded 600 s time interval. The average wind direction Φ_{av} has to fit the wind direction of interest within a tolerance of $\pm 10°$ for all time steps in the regarded 600 s. Note that the borders of the interval are including the lower limit and excluding

120 the upper limit. Since this filter only applies to the average wind direction Φ_{av}, individual wind turbines might have a slightly deviating relative wind direction for this specific time interval due to a false wind direction measurement, a yawing process which has taken place asynchronously to the majority of the other wind turbines, or a wind direction deviation due to local changes over the area of the wind farm.

As a summary, the overall filtering procedure is as follows. Each time interval of 600 consecutive seconds where the two wind

125 turbines of a wind turbine pair (as defined in Fig. 1) both fulfil all the above described filtering parameters, i.e. power range, pitch, yawing and wind direction, is used in the correlation analysis. This means that for different time intervals a different set of wind turbine pairs is considered and that furthermore, wind turbine pairs can be considered for multiple time intervals.

2.2 Correlation of power output fluctuations

Power output fluctuations of individual wind turbines are defined as deviations of the instantaneous power from the average

130 power of the regarded wind turbine i within a certain time interval Δt. We analyse time intervals of $\Delta t_{600} = 600$ s:

$$P'_{i,t_j}(t) = P_i(t) - \langle P_i(t) \rangle_{\Delta t_{600}} \tag{1}$$

where $\langle P_i(t) \rangle_{\Delta t_{600}}$ is the average of the measured power $P_i(t)$ over an interval Δt_{600} including all 600 values for t in the discretised interval $[t_j, t_j + 599 \text{ s}]$. $P'_{i,t_j}(t)$ is the power output fluctuation within the interval Δt_{600} (the index t_j is omitted in the following). Depending on the data availability, the next interval of 600 consecutive seconds could go from

135 $[t_j + 1 \text{ s}, t_j + 1 \text{ s} + 599 \text{ s}]$, and thus, partly overlap the previous one.

The selection of the interval size of 600 s is based on the layout of the wind farm and the considered power ranges with the corresponding wind speeds. For example, considering the spacing of up to 9 D for westerly winds, the cut-in wind speed of 4 ms^{-1} and rated wind speed of 12.5 ms^{-1}, a particle moving with the undisturbed wind would take from about 84 s up to

261 s to travel from one wind turbine to its downstream neighbour. Taking a lower advection wind speed within the wind

140   farm into account, a considered interval length of 600 s captures potential correlations of interest. This means, each time step

followed by 599 consecutive time steps forms an interval, individually for each wind turbine. For all available intervals of all

wind turbines, the power output fluctuations are then calculated based on Eq. 1.

To analyse the influence of wind turbines onto each other, the space-time correlation is calculated. This is done using the

Pearson correlation coefficient (Pearson, 1896)

$$r(\tau) = \frac{\langle P'_A(t) P'_B(t+\tau) \rangle_{\Delta t_{300}}}{\sqrt{\langle P'^2_A(t) \rangle_{\Delta t_{300}} \langle P'^2_B(t+\tau) \rangle_{\Delta t_{300}}}} \qquad (2)$$

where $\langle ... \rangle_{\Delta t_{300}}$ is the average over an interval $\Delta t_{300} = 300$ s including all 300 values for t in the discretised interval

$[t_j, t_j + 299 \text{ s}]$, $r(\tau)$ is the Pearson correlation coefficient in dependence of a time lag τ, $P'_A(t)$ is the power output fluctu-

ation of the upstream wind turbine A following Eq. 1 at a time t, $P'_B(t+\tau)$ is the power output fluctuation of the downstream

wind turbine B at a time $t+\tau$ with a time lag τ.

150   The Pearson correlation coefficient is a value between -1 and 1, where 1 depicts the maximum possible linear correlation, -1 is

the maximal linear anti-correlation and a value of 0 depicts no linear correlation. The correlation coefficient is evaluated for a

fixed period of 300 s from $P'_A(t)$ to $P'_A(t+300 \text{ s})$ and likewise $P'_B(t+\tau)$ to $P'_B(t+300 \text{ s}+\tau)$. This allows a maximum time

lag of $\tau = 300$ s for each considered 600 s interval.

Dependent on the wind speed, wind structures responsible for power output fluctuations measured at an upstream wind turbine

155   A take some time to travel the distance to the neighbouring downstream wind turbine B. To compare correlations at different

wind speeds and different wind turbine distances, the time lag τ is normalised for each time interval starting at t_j individually

$$\tau_{norm} = \tau \cdot \frac{\langle U_B(t) \rangle_{\Delta t_{300}}}{x_{AB}} \qquad (3)$$

where τ_{norm} is the normalized time lag, $\langle U_B(t) \rangle_{\Delta t_{300}}$ is the average wind speed measured at a certain (downstream) wind

turbine B for a time interval $\Delta t_{300} = 300$ s for t in the discretised interval $[t_j, t_j + 299 \text{ s}]$ and x_{AB} is the distance between wind

160   turbine A and wind turbine B.

The Pearson correlation coefficient in dependence of the normalised lag τ_{norm} is given as follows

$$r(\tau_{norm}) = \frac{\langle P'_A(t) P'_B(t+\tau_{norm}) \rangle_{\Delta t_{300}}}{\sqrt{\langle P'^2_A(t) \rangle_{\Delta t_{300}} \langle P'^2_B(t+\tau_{norm}) \rangle_{\Delta t_{300}}}}. \qquad (4)$$

If the average travelling velocities of the wind structures matches the average wind speed measured at wind turbine B,

$\tau_{norm} = 1$. However, in situations where wind turbine B is in the wake of wind turbine A, τ_{norm} is expected to be larger

165   than 1. The wind speed in the wake is reduced and recovers slowly, so that the wind speed measured at wind turbine B, i.e.,

U_B is already partly recovered and hence larger than the average wind speed between wind turbine A and B.

For averaging correlation curves for different wind speeds, the correlation curves are discretised using a histogram with a

reference time lag of

$$\tau_{norm,ref} = \tau \cdot \frac{U_{max}}{x_{AB}} \qquad (5)$$

where τ is the time lag (0 s to 300 s), U_{max} is an artificially introduced velocity which has to be larger than the maximum possible wind speed (since the rated wind speed is 12.5 ms^{-1}, here $U_{max} = 13$ ms^{-1}) and x_{AB} is the distance between wind turbine A and wind turbine B. Afterwards the average value of $r(\tau_{norm})$ for each bin in the histogram is calculated.

3 Wind-direction dependency and location dependency

As described in Sect. 1, the aim of this work is to study the influences of the free-field wind farm situation on space-time correlations of power output fluctuations. For that, we analyse the time intervals of a fixed set of 66 wind turbine pairs, namely those which are streamwise aligned for the wind directions 90° and 270°, see Fig. 1 and Tab. A1. Note that the pairs are the same for both wind directions but the order of the evaluation for the wind-direction dependent correlation differs (i.e. the upstream and downstream wind turbine position of a pair is reversed). In the following, we treat average correlations which relate to the correlation coefficient in Eq. 4 according to

$$R(\tau_{norm}) = \langle r(\tau_{norm}) \rangle_{all} \tag{6}$$

where $\langle ... \rangle_{all}$ is the average over a wind direction interval of 20° and all available time intervals of the considered wind turbines (either all wind turbines or a selection of wind turbines). In Sect. 3.1, the average correlation of the 66 wind turbine pairs is analysed for each wind direction interval separately. Further, in Sect. 3.2, the location-dependent correlations of the wind turbine pairs are evaluated and wind turbine statistics which characterise power output fluctuation correlations are investigated.

3.1 Wind-direction dependent space-time correlation

After applying the filters described in Sect. 2.1 to the 66 wind turbine pairs, the average correlation per wind direction is determined. For each wind turbine pair, the power output fluctuation correlations are averaged over wind direction intervals of 20° applied to steps of 10°, i.e. the interval for wind direction 90° corresponds to directions $80° \leq \Phi_{av} < 100°$ and the consecutive interval for wind direction 100° is $90° \leq \Phi_{av} < 110°$. For 10°-wind direction steps from 0° to 170° we treat the pairs according to Tab. A with reversed order and for the 10°-wind steps from 180° to 350° we treat the pairs with the given order. Afterwards, the results are averaged over all wind turbine pairs for each 10° step separately. Due to the different availability of each wind turbine pair they influence the average correlation to a different amount. Figure 2 displays the amount of data of all correlation intervals of all wind turbine pairs per wind direction interval of 20°. The main wind direction is about 220° and shows the maximum occurrence whereas 90° has about 20% less data and 270° about 45% less. For wind directions from 350° to 20° there was almost no data available. Figure 3 displays the averaged power output fluctuation correlation per 10° wind direction step (Eq. 6) which is averaged over the 20° wind direction interval and all time intervals of all available wind turbine pairs. The averaged correlation coefficient is plotted as colour and the time lag τ_{norm} (Eq. 3) as radius. For wind directions around 90° and 270° the wind turbines in a pair are streamwise aligned. Fluctuations take a certain time to travel from one wind turbine to the other where the fluctuations are influenced by the upstream wind turbine. The highest correlation peak is found to be at $\tau_{norm} > 1$ according to the definition of τ_{norm} in Eq. 3. The maximum correlation around
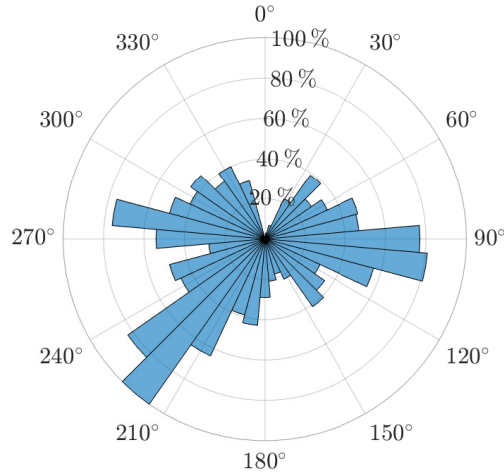
Figure 2. Availability of data per wind direction interval normalized to the number of the available correlation intervals for 220°, namely 9,102,133. The outer labels depict the wind direction and the inner circles the percentage of availability.
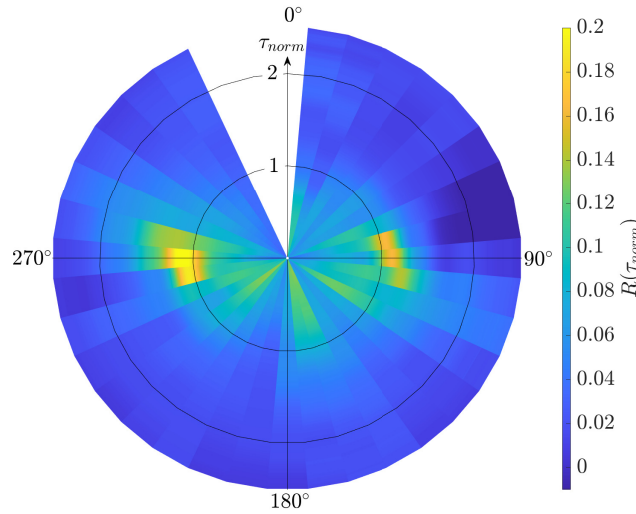
Figure 3. Average power output fluctuation correlation per 10° wind direction step of all available wind turbine pairs within the wind farm. Since the power output fluctuation correlation is averaged for wind direction intervals of 20° the intervals are overlapping by 10°. For better visibility the intervals are visualised in 10° steps only, i.e. for 90° the interval goes from 80° to 100° but is visualised from 85° to 95°. The radius of the circle is the time lag τ_{norm}, i.e. $\tau_{norm} = 0$ is in the origin, $\tau_{norm} = 1$ is on the inner black circle. No data was available for the wind direction interval around 350° (cf. Fig. 2).

0.2 may seem rather low but is reasonable considering the high variability in the flow and wind turbine dynamics in free-field measurements. For wind directions approaching 0° and 180° the wind turbines in a pair are oriented more perpendicular to the wind. Fluctuations reach the downstream turbine earlier. This leads to a change in the expected position of the highest peak and
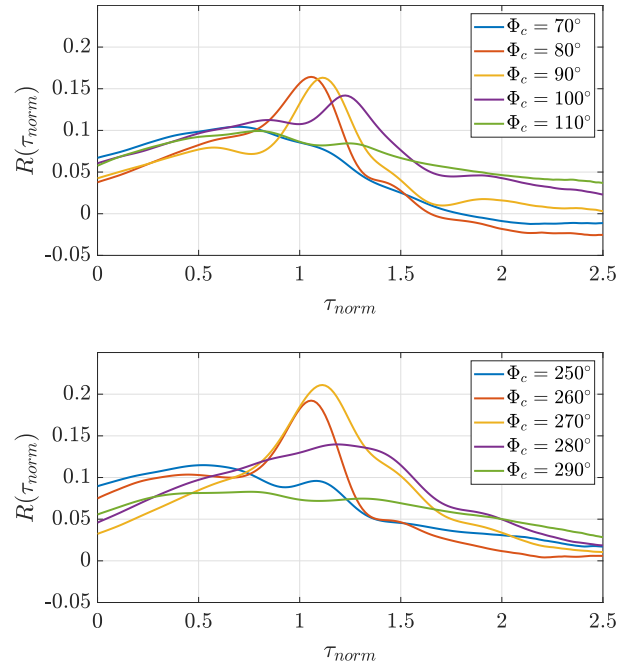
Figure 4. Average power output fluctuation correlations for wind direction intervals from around 70° to 110° and around 250° to 290° as radial cuts through Fig. 3. Φ_c depicts the centre of the wind direction intervals.

the peak magnitude. The correlation is not as pronounced as for the streamwise case above (i.e. around 90° and 270°) which

205 confirms simulation results by Stevens and Meneveau (2014). We will not investigate the spanwise correlations in further detail here. Figure 4 shows the average power output fluctuation correlation around 90° and 270° as cuts through Fig. 3 in detail. The absolute peaks are at 90° and 270°. For wind directions where the wind turbines in a pair are less streamwise aligned the peak decreases and the correlation curve flattens. In contrast to 90°, the correlations for 270° are more defined and show slightly larger peak values. This maybe due to the non-axisymmetric wind farm layout (cf. Fig. 1).

210 ## 3.2 Location-dependent space-time correlation

The location dependency of the averaged power output fluctuation correlations is investigated for wind directions 90° and 270°. As mentioned before, for these two wind directions the wind turbines are streamwise aligned. The most northern wind turbines 1 to 8, and wind turbines 58 to 80 in the lower triangle of the wind farm, do not follow the symmetric pattern of the square consisting of wind turbines 9 to 57. The following results are limited to this symmetric square marked in Fig. 1.

215 Figure 5 displays the averaged correlations of the power output fluctuations for all wind turbine pairs included in the upper square of the wind farm for the wind directions 90° and 270°, respectively. For 90°, in total 4,916,277 intervals of 600 s are averaged while for 270° the number of 600 s-intervals is 3,329,333. Similar to Fig. 4, both correlation curves show a comparable shape whereas the correlation for 270° is in general higher than for 90°. For 90°, the maximum averaged correlation coefficient

WIND
ENERGY
SCIENCE
DISCUSSIONS

eawe
european academy of wind energy
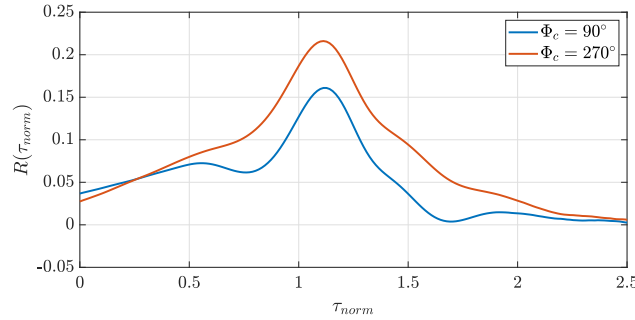
Figure 5. Average power output fluctuation correlation for wind direction intervals around 90° and 270° considering the wind turbines 9 to 57 in the symmetric square (cf. Fig. 1). Φ_c depicts the centre of the wind direction intervals.

is about 0.16, for 270° it is about 0.21.

220   To further analyse the flow and wake situation, we determine the average standard deviation of the power output fluctuations and the average normalised power difference of the upstream and downstream wind turbines. The results for 90° and 270° are listed in Tab. 2. For both wind directions the averaged standard deviation of the power output fluctuations is larger for the downstream wind turbine than for the upstream one. In general, however, the averaged standard deviation of the power output fluctuations for 90° is smaller than for 270°. Further, the normalised power difference of the wind turbines for 90° is about 12%

225   and for 270° about 8%. The different behaviour is likely to be caused by distinct meteorological conditions, e.g. distribution of mean wind speed and atmospheric stability, between the two wind directions. To further investigate the wind turbine location dependency of the power output fluctuation correlations, the average correlation of wind turbine rows is calculated for both wind directions. Here, a wind turbine row consists of a line of wind turbines perpendicular to the incoming wind as shown in the upper right corner of Fig. 6. For both wind directions no sharp correlation is found for the first row (turbine A in the first

230   row, turbine B downstream of A, dark blue curves). It has to be marked that the upstream wind turbine A is standing in free stream while the downstream wind turbine B is affected by the wake of the upstream wind turbine. Thus, the two wind turbines

Table 2. Averaged wind turbine statistics computed for wind direction intervals around 90° and 270° with A as upstream wind turbine and B as downstream wind turbine. $\sqrt{\langle P_A'^2 \rangle_{\Delta t_{600}}}$ is the standard deviation of the power output fluctuations of wind turbine A over 600 s intervals Δt_{600} (analogue for wind turbine B for the same 600 s intervals, respectively). $\langle P_A \rangle_{\Delta t_{600}}$ and $\langle P_B \rangle_{\Delta t_{600}}$ are the average power of wind turbines A and B over the same 600 s intervals. $\langle ... \rangle_{all}$ denotes the average of the statistics over all available time intervals of the wind turbine pairs. Note that Φ_c depicts the centre of 20° wind direction intervals, here from 80° to 100° and from 260° to 280°.

Φ_c	$\left\langle \sqrt{\langle P_A'^2 \rangle_{\Delta t_{600}}} \right\rangle_{all}$ [kW]	$\left\langle \sqrt{\langle P_B'^2 \rangle_{\Delta t_{600}}} \right\rangle_{all}$ [kW]	$\left\langle \frac{\langle P_A \rangle_{\Delta t_{600}} - \langle P_B \rangle_{\Delta t_{600}}}{\langle P_A \rangle_{\Delta t_{600}}} \right\rangle_{all}$
90°	211.91	221.92	0.123
270°	246.54	260.29	0.080
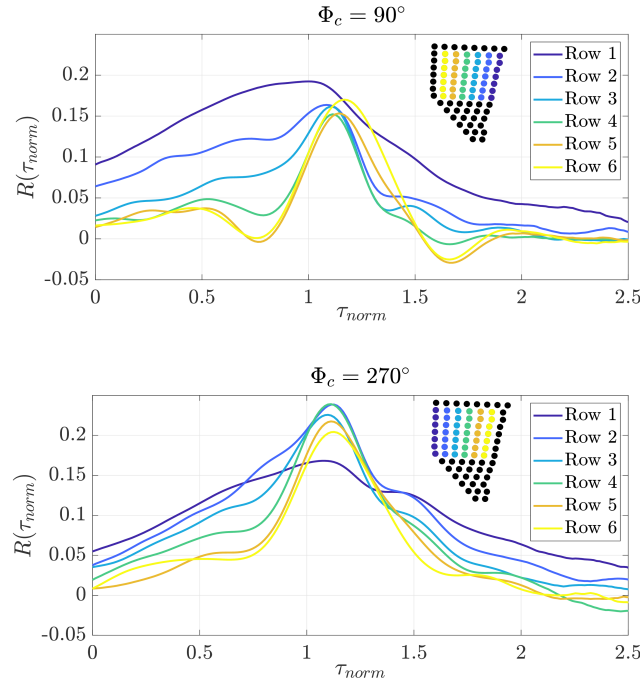
Figure 6. Averaged power output fluctuation correlation for wind direction intervals around 90° (top) and 270° (bottom) considering all wind turbines in the symmetric square (cf. Fig. 1). Φ_c depicts the centre of the wind direction intervals. $R(\tau_{norm})$ is calculated by Eq. 6 where turbine A is located in the respective coloured row and turbine B is one row downstream of A. As the wind turbines are analysed in pairs of two, the last row of wind turbines is unlabelled as these wind turbines do not have a downstream partner. For both figures the numbers and colours are identical with regard to the considered wind direction.

have very different inflow conditions. For wind turbine pairs further downstream both wind turbines are standing in the wake of upstream wind turbines. Here, a clear correlation is found. For the second to last row, the peaks become more defined as their width decreases.

235   As described by Bossuyt et al. (2017a), the turbulence intensity increases with the flow towards the back of the wind farm. Furthermore, as indicated above in Lukassen et al. (2018), the variance of wind speed fluctuations plays an important role in modelling the velocity space-time correlations. To evaluate the row-dependent conditions in the measurement data, Tab. 3 lists the average standard deviations of the power output fluctuations measured at the upstream and downstream wind turbine of all pairs as well as the average normalised power difference of all pairs. For both wind turbines in a pair, the average standard

240   deviations of the power output fluctuations show a clear increasing trend throughout the wind farm, similar to the turbulence intensity in the wind tunnel results mentioned above. The normalised power difference is largest for the first row which is caused by the previously described deviating inflow conditions of the upstream and downstream wind turbines. This was also found in the experiment by Bossuyt et al. (2017a) where the first row generates the maximum power, the second and following rows show a significant reduction.

Table 3. Averaged wind turbine statistics per wind farm row computed for wind direction intervals around 90° and 270° with A as upstream wind turbine and B as downstream wind turbine. $\sqrt{\langle P_A'^2 \rangle_{\Delta t_{600}}}$ is the standard deviation of the power output fluctuations of wind turbine A over a 600 s interval Δt_{600} (analogue for wind turbine B for the same 600 s intervals, respectively). $\langle P_A \rangle_{\Delta t_{600}}$ and $\langle P_B \rangle_{\Delta t_{600}}$ are the average power outputs of wind turbines A and B over the same 600 s intervals. $\langle ... \rangle_{row}$ denotes the average of the statistics over all available time intervals of the wind turbine pairs in a row. Note that 90° and 270° again refer to 20° wind direction intervals from 80° to 100° and from 260° to 280°.

	$\left\langle \sqrt{\langle P_A'^2 \rangle_{\Delta t_{600}}} \right\rangle_{row}$ [kW]		$\left\langle \sqrt{\langle P_B'^2 \rangle_{\Delta t_{600}}} \right\rangle_{row}$ [kW]		$\left\langle \frac{\langle P_A \rangle_{\Delta t_{600}} - \langle P_B \rangle_{\Delta t_{600}}}{\langle P_A \rangle_{\Delta t_{600}}} \right\rangle_{row}$	
Row	90°	270°	90°	270°	90°	270°
1	113.90	166.49	164.19	216.16	0.269	0.188
2	186.13	232.31	221.54	257.82	0.051	0.015
3	223.71	253.71	241.92	265.01	0.091	0.060
4	242.84	268.60	240.76	267.94	0.097	0.059
5	249.78	275.55	234.00	274.45	0.075	0.076
6	232.14	280.34	219.92	277.82	0.058	0.038

4 K-means clustering of power output fluctuation characteristics

The results of section 3.2 reveal that the standard deviation of the power output fluctuations as well as the power difference of the wind turbines change depending on the location of the wind turbine (pairs) within the wind farm. As explained in section 2.1, conditions in a wind farm are never ideal due to the variety of influence factors such as wind direction and wind speed fluctuations or influences of surrounding wind turbines. Turbines within the wind farm which are turned off or derated might create free-stream like inflows for downstream wind turbine pairs. Such irregularities might influence the standard deviations and power differences calculated for the wind turbine pairs. Even though such wind turbines are filtered out for the analysis, they still influence the surrounding wind turbines in an unpredictable way. To identify these locally abnormal conditions and the resulting deviations in the power output fluctuations and their correlations, the k-means clustering algorithm is used to sort the correlations based on the previously defined statistics of the power output fluctuations, namely the standard deviation and the normalised power difference. In the following, we investigate these influences for the directions 90° and 270°. Furthermore, the triangular shape of the lower part of the wind farm (wind turbines 58 to 80) as well as the most northern wind turbines 1 to 8 are incorporated now (cf. Fig. 1) to identify the flow conditions there. This results in 6,985,830 considered time intervals for 90° and 4,914,448 considered time intervals for 270°. Figure 7 is the pendant to Fig. 5 showing the average correlations for 90° and 270° for all available wind turbine pairs in the whole wind farm. Even though this plot looks very similar to Fig. 5, it does not show the same content. Note that the blue curve is the same curve as for 90° in Fig. 4 and the orange curve is the same curve as for 270° in Fig. 4. The clustering is performed using the k-means algorithm of MATLAB (MATLAB, 2019) based on Lloyd (1982), using random sample points as initial centroids, the squared euclidean distance as distance metric, with
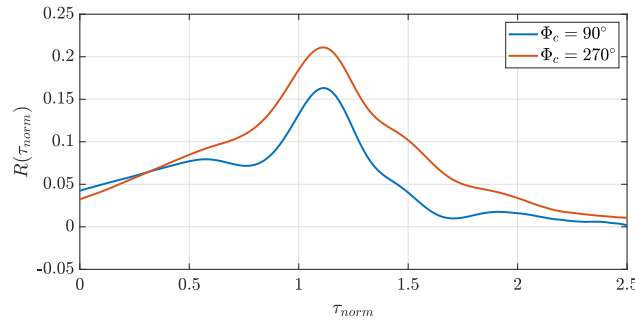
Figure 7. Averaged power output fluctuation correlation for wind direction intervals around 90° and 270° considering all available wind turbine pairs in the whole wind farm and all available time intervals. Φ_c depicts the centre of the wind direction intervals. $R(\tau_{norm})$ is computed according to Eq. 6.

a maximum of 300 iterations and five clusters. The number of the clusters was empirically chosen as the data was grouped into a reasonable set of groups and a greater number of cluster did not lead to further clusters of importance for the present
265 analysis (see appendix B). To avoid the generation of local centroids the clustering is repeated ten times and the run with the clusters with the lowest sum of point-to-centroid distances within the clusters is chosen. Different orderings of the intervals have been tested, namely random sorting, data sorted for increasing standard deviation of the downstream wind turbine B, and a chronological sorting according to the available time intervals. The results have been found to be equal including the first decimal place of the centroids for all cases, thus, the random sorting is used in the further analysis.

270 Table 4 lists the centroids (centres of the clusters). The standard deviations of both wind turbines A and B are significantly decreasing while the normalised power difference of A and B is significantly increasing from cluster 1 to 5. To further investigate these findings, we analyse the correlation curves corresponding to the clusters. Figures 8 and 9 show the average correlations for both wind directions for each of the five clusters (upper plots) and the percentage frequency of each pair within each of the five clusters (lower plots). As expected from Fig. 7, the average correlations for 270° are higher than for 90°. Cluster 1
275 includes nearly 6% of the data and has the highest correlation. This is a significant increase compared to the average correlation shown in Fig. 7. From cluster 2 to 4 the correlation is decreasing while the amount of data per cluster increases. For cluster 5 no correlation is found. Looking at the occurrence of wind turbine pairs within each cluster, a clear trend is visible. While cluster 1 with the highest correlation is dominated by wind turbine pairs where the upstream wind turbine is located towards the back of the wind farm, cluster 5 with no correlation is dominated by wind turbine pairs with its upstream wind turbine located in
280 the first row of the wind farm. From Cluster 2 to 4 the dominating wind turbine pairs shift from the back rows towards the front rows whereas the percentage frequency become mores balanced throughout the wind farm (i.e. more light green coloured turbines).

Comparison of the results of Fig. 8 and 9 and Tab. 4 clearly depicts that the greater the standard deviations and the smaller the normalised power difference the higher the correlation of the wind turbine pairs. The slight row dependence which was already
285 indicated in Tab. 3 can be confirmed here. This is illustrated by a colour coding of frequency of occurrence of wind turbine

Table 4. Cluster centroids for wind direction intervals around 90° and 270° with A as upstream wind turbine and B as downstream wind turbine. $\sqrt{\langle P_A'^2 \rangle_{\Delta t_{600}}}$ is the standard deviation of the power outputs fluctuations of wind turbine A over 600 s intervals Δt_{600} (analogue for wind turbine B for the same 600 s intervals, respectively). $\langle P_A \rangle_{\Delta t_{600}}$ and $\langle P_B \rangle_{\Delta t_{600}}$ are the average power output of wind turbines A and B over the same 600 s intervals. $\langle ... \rangle_{cluster}$ denotes the average of the statistics over all available time intervals of the wind turbine pairs within a cluster. Note that 90° and 270° again refer to 20° wind direction intervals from 80° to 100° and from 260° to 280°.

	$\left\langle \sqrt{\langle P_A'^2 \rangle_{\Delta t_{600}}} \right\rangle_{cluster}$ [kW]		$\left\langle \sqrt{\langle P_B'^2 \rangle_{\Delta t_{600}}} \right\rangle_{cluster}$ [kW]		$\left\langle \frac{\langle P_A \rangle_{\Delta t_{600}} - \langle P_B \rangle_{\Delta t_{600}}}{\langle P_A \rangle_{\Delta t_{600}}} \right\rangle_{cluster}$	
Cluster	90°	270°	90°	270°	90°	270°
1	512.62	534.80	526.57	539.96	0.015	0.046
2	366.52	381.35	386.56	405.02	0.049	0.057
3	252.95	283.41	270.62	297.57	0.103	0.060
4	156.91	196.58	173.92	213.27	0.128	0.072
5	73.31	116.88	85.60	133.12	0.140	0.108
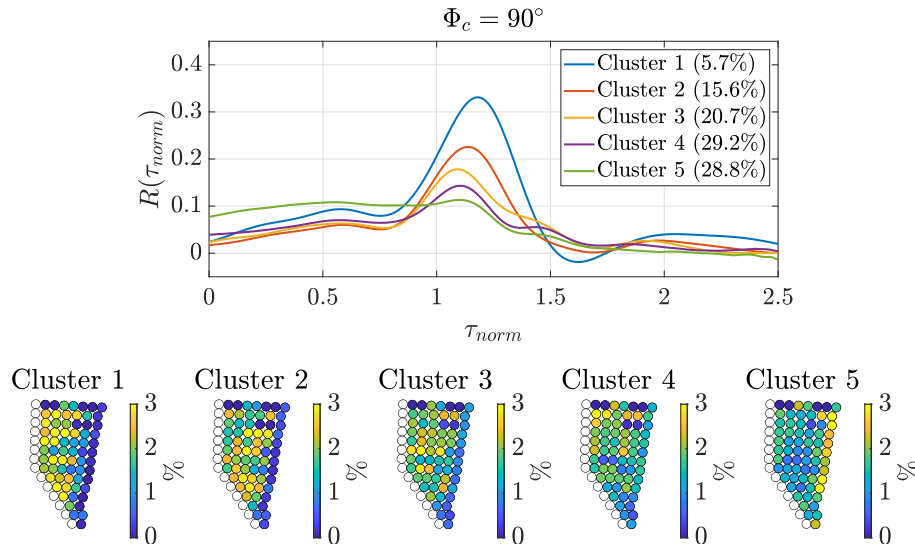
Figure 8. Clustering for wind direction interval around 90° with randomly sorted 600 s time intervals. Φ_c depicts the centre of the wind direction interval. The upper plot shows the average power output fluctuation correlation curve per cluster. The legend lists the share of data. The lower plot shows the percentage frequency of each wind turbine pair within the respective cluster given as colour. As the wind turbines are analysed in pairs of two, the last row of wind turbines is unlabelled as these wind turbines do not have a downstream partner.

pairs in each cluster in the lower subplot of Fig. 8 (respectively Fig. 9). The sum of all frequencies of all wind turbines within one cluster add up to 100% meaning a yellow coloured wind turbine pair makes up about 3% of the respective cluster and a green marked wind turbine pair makes up about 1.5% of the respective cluster. For example, the correlation peak for cluster 1
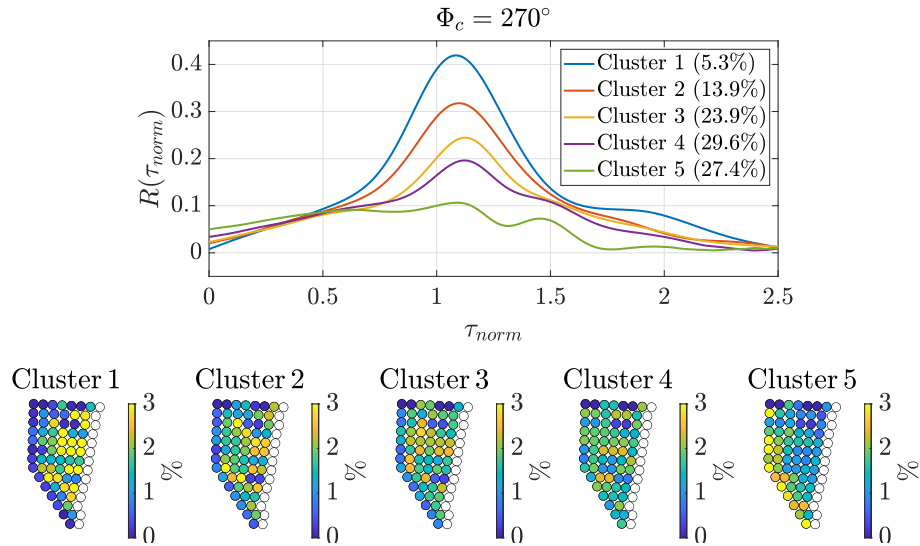
Figure 9. Clustering for wind direction interval around 270° with randomly sorted 600 s time intervals. Φ_c depicts the centre of the wind direction interval. The upper plot shows the average power output fluctuation correlation curve per cluster. The legend lists the share of data. Note that the values do not add up exactly to 100% due to rounding. The lower plot shows the percentage frequency of each wind turbine pair within the respective cluster given as colour. As the wind turbines are analysed in pairs of two, the last row of wind turbines is unlabelled as these wind turbines do not have a downstream partner.

of more than 0.3 for 90° (respectively 0.4 for 270°) partly includes pairs with the upstream turbine in the last row but also some
290   turbine pairs in the rows before. This is considerably larger than the correlation curve of row 6 of Fig. 6.

5   Conclusions

An analysis of power output fluctuations based on high resolution SCADA data of an offshore wind farm was conducted. For measurements from 80 wind turbines, a filtering was applied to create a data set of less variability and a quasi-steady flow condition. For the filtered data, the power output fluctuations were calculated for time intervals of 600 s. In the next step the
295   correlation of the power output fluctuations of wind turbine pairs was evaluated using the Pearson correlation coefficient. Streamwise aligned pairs showed the highest correlation. Deviations from the 90° and 270° wind directions result in a decreased correlation. After analysing the average correlation in dependence of the wind direction, the correlation for the wind directions of 90° and 270° were investigated in detail. Determining the average correlation per row within the wind farm showed that the correlation changes throughout the wind farm. Pairs with the upstream turbines in the first row of the wind
300   farm display no correlation due to the free-stream situation of the upstream wind turbines. The further down in the wind farm, the more defined were the correlations. Moreover, based on the findings of Bossuyt et al. (2017a) which showed an increasing turbulence intensity throughout the wind farm and the model for velocity space-time correlations by Lukassen et al. (2018),

statistics characterising the power output fluctuations were defined and evaluated. The standard deviation of the upstream and downstream wind turbine in a pair as well as the normalised power difference of the wind turbines were chosen for charac-

305   terisation. The analysis of the separate rows of the wind farm revealed a trend of increasing standard deviations throughout the wind farm and decreasing power difference. Due to the high variability in the flow throughout the wind farm, not all wind turbine pairs in the same row are affected by the same flow conditions. Thus, the clustering algorithm k-means was used to group the correlations based on the previously defined statistics.

The outcome of the clustering is that the chosen wind turbine statistics allow to characterise the power output fluctuation

310   correlations. Increased standard deviations combined with small power differences show the highest correlations which tend to increase downstream in the wind farm. For both wind directions a cluster with a significantly increased average correlation from 0.16 to 0.32 for 90° and from 0.21 to 0.41 for 270° was found.

As an outlook, further analysis on the space-time correlations within an offshore wind farm could help in the control of wind turbines, e.g. for power output fluctuation management or active wake control. Also, knowledge about the correlation of wind

315   turbine pairs allows short-term power output fluctuation forecast within the wind farm as well as interactive wind turbine control.

The presented findings can be enhanced in the future by additional Lidar or Radar measurements to access independent wind direction and wind speed measurements. Also the analysis of correlations might be extended to include the correlation of wind turbine pairs with multiple inter-turbine distances and the correlation of non-aligned wind turbine pairs. The clustering of

320   correlation states can be further investigated by increasing the number of clusters to $k > 5$ as the results for $k = 6$ indicated that the statistics of the upstream and downstream wind turbine of a pair has different influence on its correlation. Also, it is worth considering alternative clustering methods like k-medoids (Kaufman and Rousseeuw, 2008) or Density-Based Spatial Clustering of Applications with Noise (DBSCAN) (Ester et al., 1996). Furthermore, measurements on the boundary layer conditions help to assess the influence of wind turbine wakes on the space-time correlations of power output fluctuations with

325   the additional knowledge on the atmospheric stability.

Appendix A: Wind turbine pairs

In order to calculate the power output fluctuation correlation, wind turbine pairs are chosen according to the respective wind direction. In total, 66 wind turbine streamwise pairs can be defined. Table A1 depicts the definition of wind turbine pairs for wind directions 270°. For wind direction 90°, the same pairs are chosen but with switched wind turbine order. E.g. for pair 1 for 270°, wind turbine 1 is the upstream wind turbine and turbine 2 is the downstream wind turbine, respectively for 90°, wind turbine 2 is the upstream wind turbine and turbine 1 is the downstream wind turbine.

Table A1. Definition of streamwise wind turbine pairs for wind direction 270°.

Pair	01	02	03	04	05	06	07	08	09	10	11	12	13	14
WTs	01, 02	02, 03	03, 04	04, 05	05, 06	06, 07	07, 08	09, 10	10, 11	11, 12	12, 13	13, 14	14, 15	16, 17

Pair	15	16	17	18	19	20	21	22	23	24	25	26	27	28
WTs	17, 18	18, 19	19, 20	20, 21	21, 22	23, 24	24, 25	25, 26	26, 27	27, 28	28, 29	30, 31	31, 32	32, 33

Pair	29	30	31	32	33	34	35	36	37	38	39	40	41	42
WTs	33, 34	34, 35	35, 36	37, 38	38, 39	39, 40	40, 41	41, 42	42, 43	44, 45	45, 46	46, 47	47, 48	48, 49

Pair	43	44	45	46	47	48	49	50	51	52	53	54	55	56
WTs	49, 50	51, 52	52, 53	53, 54	54, 55	55, 56	56, 57	58, 59	59, 60	60, 61	61, 62	62, 63	64, 65	65, 66

Pair	57	58	59	60	61	62	63	64	65	66
WTs	66, 67	67, 68	69, 70	70, 71	71, 72	73, 74	74, 75	76, 77	77, 78	79, 80

Appendix B: Effect of the numbers of clusters

As mentioned in Sect. 4, the number of clusters chosen for the present analysis was k = 5. This decision was made based on the results for k = 6, as an increasing number of clusters revealed further features outside of the scope of this work. Figure B1 and Fig. B2 present the clustering results for k = 6. For wind direction 90°, six clearly separable correlation curves are found. Cluster 2 shows an abnormal characteristic compared to cluster 1 and 3 as here, mostly wind turbines in the second and third row are dominating the cluster. The result for wind direction 270° are 4 clearly separable correlation curves and two very similar ones. Cluster 3 displays an abnormal characteristics compared to cluster 2 and 4 as here, again wind turbines from the second row are dominating the cluster. Looking at the statistics of the correlation curves listed in Tab. B1 it further can be found that the standard deviation of the upstream and downstream wind turbines influences the correlation curves differently. For wind direction 90°, cluster 2 and 3 have a different order in the standard deviation of the power output fluctuation of wind turbine A and B. While the average standard deviation of the downstream wind turbine B is decreasing from cluster 2 to cluster 3, the average standard deviation of the upstream wind turbine A is higher for cluster 3 than for cluster 2. The same is found for wind direction 270°. The average standard deviation of the downstream wind turbine B is decreasing from cluster 3 to cluster
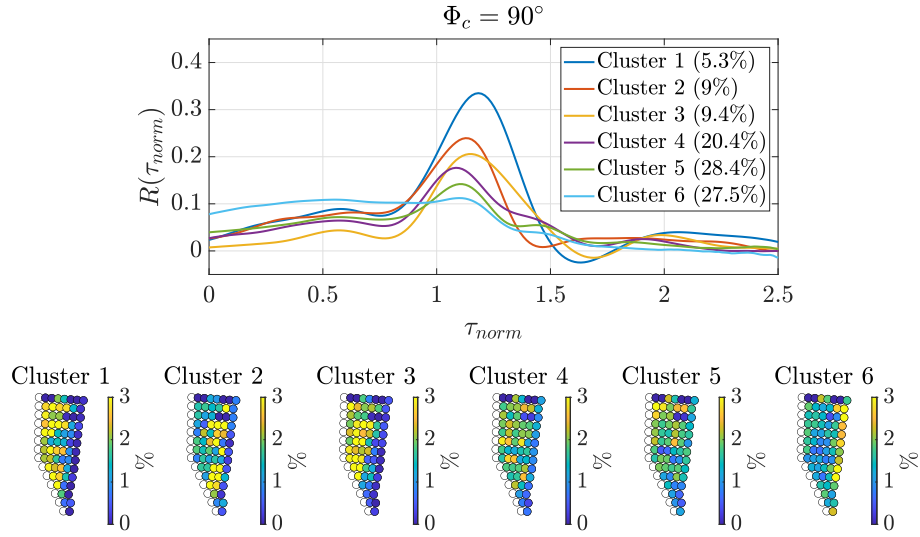
Figure B1. Clustering for wind direction interval around 90° with randomly sorted parameters and $k = 6$. Φ_c depicts the centre of the wind direction interval.

Table B1. Averaged wind turbine statistics computed for wind direction intervals around 90° and 270° and k = 6, with A as upstream wind turbine and B as downstream wind turbine. $\sqrt{\langle P_A'^2 \rangle_{\Delta t_{600}}}$ is the standard deviation of the power output fluctuations of wind turbine A over a 600 s interval Δt_{600} (analogue for wind turbine B for the same 600 s intervals, respectively). $\langle P_A \rangle_{\Delta t_{600}}$ and $\langle P_B \rangle_{\Delta t_{600}}$ are the average power of wind turbines A and B over the same 600 s intervals. $\langle ... \rangle_{cluster}$ denotes the average of the statistics over all available time intervals of the wind turbine pairs. Note that here 90° and 270° again refer to 20° wind direction intervals from 80° to 100° and from 260° to 280°.

	$\left\langle \sqrt{\langle P_A'^2 \rangle_{\Delta t_{600}}} \right\rangle_{cluster}$ [kW]		$\left\langle \sqrt{\langle P_B'^2 \rangle_{\Delta t_{600}}} \right\rangle_{cluster}$ [kW]		$\left\langle \frac{\langle P_A \rangle_{\Delta t_{600}} - \langle P_B \rangle_{\Delta t_{600}}}{\langle P_A \rangle_{\Delta t_{600}}} \right\rangle_{cluster}$	
Cluster	90°	270°	90°	270°	90°	270°
1	522.59	540.78	526.30	547.28	0.015	0.044
2	327.11	393.94	435.21	411.84	0.024	0.055
3	393.39	246.96	323.89	342.78	0.086	0.056
4	239.51	317.42	263.24	263.02	0.105	0.068
5	152.34	194.22	168.26	210.90	0.129	0.072
6	71.53	115.92	83.59	132.18	0.140	0.109

345 4, the average standard deviation of the upstream wind turbine A is higher for cluster 4 than for cluster 3.

This implies that a further separation of the statistics with $k > 5$ might result in a distinction of the effect of the upstream and downstream wind turbine of the correlation a pair. This is here not further investigated as this effect is not included in the scope of the work presented here.
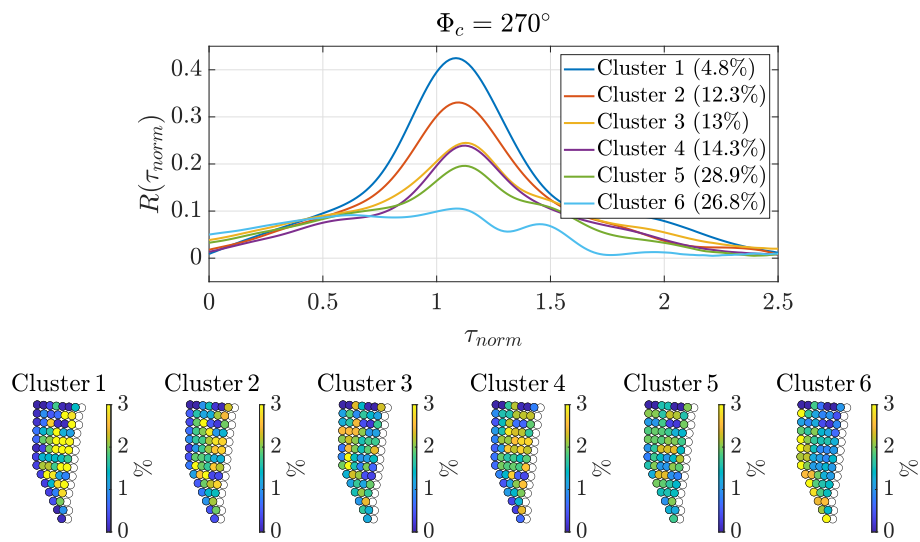
Figure B2. Clustering for wind direction interval around 270° with randomly sorted parameters and $k = 6$. Φ_c depicts the centre of the wind direction interval.

Author contributions. JKS developed the underlying method, performed the data analyses and wrote the paper. LJL provided intensive
350 consultation on the development of the method and the scientific analyses. MKr and MKü provided intensive reviews on the scientific
analyses. LJL had a supervising function.

Competing interests. The authors declare that they have no conflict of interest.

Acknowledgements. We performed parts of the work within the research project "OWP Control" (FKZ 0324131A) funded by the German
Ministry of Economic Affairs and Energy basis of a decision by the German Bundestag. Parts of the computations were performed on the
355 high performance computing system EDDY of the University of Oldenburg founded by the Federal Ministry of Economic Affairs and Energy.
We acknowledge the wind farm operator Global Tech I Offshore Wind GmbH for providing SCADA data and their support of the work.

References

Andersen, S. J., Sørensen, J. N., and Mikkelsen, R. F.: Turbulence and entrainment length scales in large wind farms, Philosophical Transactions of the Royal Society A: Mathematical, Physical and Engineering Sciences, 375, 20160 107, https://doi.org/10.1098/rsta.2016.0107, 2017.

Bossuyt, J., Howland, M. F., Meneveau, C., and Meyers, J.: Measurement of unsteady loading and power output variability in a micro wind farm model in a wind tunnel., Experiments in Fluids, 58, 1–17, https://doi.org/10.1007/s00348-016-2278-6, 2017a.

Bossuyt, J., Meneveau, C., and Meyers, J.: Wind farm power fluctuations and spatial sampling of turbulent boundary layers, Journal of Fluid Mechanics, 823, 329–344, https://doi.org/10.1017/jfm.2017.328, 2017b.

Braun, T., Waechter, M., Peinke, J., and Guhr, T.: Correlated power time series of individual wind turbines: A data driven model approach, Journal of Renewable and Sustainable Energy, 12, 023 301, https://doi.org/10.1063/1.5139039, 2020.

Bromm, M., Rott, A., Beck, H., Vollmer, L., Steinfeld, G., and Kühn, M.: Field investigation on the influence of yaw misalignment on the propagation of wind turbine wakes, Wind Energy, 21, 1011–1028, https://doi.org/10.1002/we.2210.

Crespo, A. and Hernàndez, J.: Turbulence characteristics in wind-turbine wakes, Journal of Wind Engineering and Industrial Aerodynamics, 61, 71 – 85, https://doi.org/10.1016/0167-6105(95)00033-X, 1996.

Dai, J., Cao, J., Liu, D., Wen, L., and Long, X.: Power fluctuation evaluation of large-scale wind turbines based on SCADA data, IET Renewable Power Generation, 11, 395–402, https://doi.org/10.1049/iet-rpg.2016.0124, 2017.

Ester, M., Kriegel, H.-P., Sander, J., and Xu, X.: A Density-Based Algorithm for Discovering Clusters in Large Spatial Databases with Noise, in: Proceedings of the Second International Conference on Knowledge Discovery and Data Mining, KDD'96, p. 226–231, AAAI Press, 1996.

Kaufman, L. and Rousseeuw, P.: Partitioning Around Medoids (Program PAM), chap. 2, pp. 68–125, John Wiley & Sons, Ltd, https://doi.org/10.1002/9780470316801.ch2, 2008.

Lloyd, S. P.: Least squares quantization in PCM, IEEE Transactions on Information Theory, 28, 129–137, https://doi.org/10.1002/9780470316801.ch2, 1982.

Lukassen, L. J., Stevens, R. J. A. M., Meneveau, C., and Wilczek, M.: Modeling space-time correlations of velocity fluctuations in wind farms, Wind Energy, 21, 474–487, https://doi.org/10.1002/we.2172, 2018.

MATLAB: version 9.7.0.1190202 (R2019b), The MathWorks Inc., Natick, Massachusetts, 2019.

Pearson, K.: Mathematical Contributions to the Theory of Evolution. III. Regression, Heredity, and Panmixia, Philosophical Transactions of the Royal Society A: Mathematical, Physical and Engineering Sciences, 187, 253–318, https://doi.org/10.1098/rsta.1896.0007, 1896.

Porté-Agel, F., Bastankhah, M., and Shamsoddin, S.: Wind-Turbine and Wind-Farm Flows: A Review, Boundary-Layer Meteorology, 174, https://doi.org/10.1007/s10546-019-00473-0, 2020.

Ren, G., Liu, J., Wan, J., Guo, Y., and Yu, D.: Overview of wind power intermittency: Impacts, measurements, and mitigation solutions, Applied Energy, 204, 47 – 65, https://doi.org/10.1016/j.apenergy.2017.06.098, 2017.

Sanchez Gomez, M. and Lundquist, J. K.: The effect of wind direction shear on turbine performance in a wind farm in central Iowa, Wind Energy Science, 5, 125–139, https://doi.org/10.5194/wes-5-125-2020, 2020.

Schneemann, J., Rott, A., Dörenkämper, M., Steinfeld, G., and Kühn, M.: Cluster wakes impact on a far-distant offshore wind farm's power, Wind Energy Science, 5, 29–49, https://doi.org/10.5194/wes-5-29-2020, 2020.

Sorensen, P., Cutululis, N. A., Vigueras-Rodriguez, A., Jensen, L. E., Hjerrild, J., Donovan, M. H., and Madsen, H.: Power Fluctuations From Large Wind Farms, IEEE Transactions on Power Systems, 22, 958–965, https://doi.org/10.1109/TPWRS.2007.901615, 2007.

395 Stevens, R. J. A. M. and Meneveau, C.: Temporal structure of aggregate power fluctuations in large-eddy simulations of extended wind-farms, Journal of Renewable and Sustainable Energy, 6, 043 102, https://doi.org/10.1063/1.4885114, 2014.

Vali, M., Petrović, V., Steinfeld, G., Y. Pao, L., and Kühn, M.: An active power control approach for wake-induced load alleviation in a fully developed wind farm boundary layer, Wind Energy Science, 4, 139–161, https://doi.org/10.5194/wes-4-139-2019, 2019.

Valldecabres, L., von Bremen, L., and Kühn, M.: Minute-Scale Detection and Probabilistic Prediction of Offshore Wind Turbine Power
400 Ramps using Dual-Doppler Radar, https://doi.org/10.5194/wes-3-869-2018, 2020.

Vermeer, L., Sørensen, J., and Crespo, A.: Wind turbine wake aerodynamics, Progress in Aerospace Sciences, 39, 467 – 510, https://doi.org/10.1016/S0376-0421(03)00078-2, 2003.

WindEurope: Wind energy in Europe in 2019, Tech. rep., WindEurope, Brussels, Belgium, 2020a.

WindEurope: Offshore Wind in Europe, Tech. rep., WindEurope, Brussels, Belgium, 2020b.